INTERNATIONAL JOURNAL FOR NUMERICAL METHODS IN BIOMEDICAL ENGINEERING
Int. J. Numer. Meth. Biomed. Engng. 0000; **00**:1–26
Published online in Wiley InterScience (www.interscience.wiley.com). DOI: 10.1002/cnm

Effects of walking in deep venous thrombosis: a new integrated solid and fluid mechanics model

Josep M. López[1*], Gerard Fortuny[1], Dolors Puigjaner[1], Joan Herrero[2], Francesc Marimon[3] and Josep Garcia–Bennett[4]

[1]*Departament d'Enginyeria Informàtica i Matemàtiques, Universitat Rovira i Virgili, Av Països Catalans 26, Tarragona, Catalunya, Spain*
[2]*Departament d'Enginyeria Química, Universitat Rovira i Virgili, Av Països Catalans 26, Tarragona, Catalunya, Spain*
[3]*Departament de Medicina i Cirurgia, Universitat Rovira i Virgili, Hospital Sant Joan, Reus, Catalunya, Spain*
[4]*Servei de Radiologia i Diagnòstic per la Imatge, Hospital Sant Joan, Reus, Catalunya, Spain*

SUMMARY

Deep venous thrombosis (DVT) is a common disease. Large thrombi in venous vessels cause bad blood circulation and pain; and when a blood clot detaches from a vein wall, it causes an embolism whose consequences range from mild to fatal. Walking is recommended to DVT patients as a therapeutical complement. In this study the mechanical effects of walking on a specific patient of DVT were simulated by means of an unprecedented integration of three elements: a real geometry, a biomechanical model of body tissues and a computational fluid dynamics (CFD) study. A set of computerized tomography (CT) images of a patient's leg with a thrombus in the popliteal vein was employed to reconstruct a geometry model. Then a biomechanical model was used to compute the new deformed geometry of the vein as a function of the fiber stretch level of the semimembranosus muscle. Finally, a CFD study was carried out in order to compute the blood flow and the wall shear stress (WSS) at the vein and thrombus walls. Calculations showed that either a lengthening or shortening of the semimembranosus muscle led to a decrease of WSS levels up to a 10%. Notwithstanding, changes in blood viscosity properties or blood flow rate may easily have a greater impact in WSS.

Received ...

KEY WORDS: International standard thrombotic treatment; Computational fluid dynamics; Deep venous thrombosis; Biomechanical model; Wall shear stress

1. INTRODUCTION

Deep venous thrombosis (DVT) takes place when blood clots, which are called thrombi, form inside one of the deep veins and interfere in the normal blood circulation. DVT can cause post–thrombotic syndrome with chronic pain and leg swelling that restrict the patient's mobility. But DVT can result

*Correspondence to: Departament d'Enginyeria Informàtica i Matemàtiques, Universitat Rovira i Virgili, Av Països Catalans 26, Tarragona, Catalunya, Spain. E-mail:josep.m.lopez@urv.cat

in much more devastating effects or even death if a clot or parts of it detach and travel through the venous system [1]. A clot that travels through the bloodstream is called a thrombo–embolus and if it becomes lodged somewhere in the pulmonary vascular system it can cause an embolism. Ischemic injury, infarction, and necrosis of the tissues in the affected area are some of the possible consequences of embolisms. Venous thromboembolism is a disease that includes both DVT and pulmonary embolism. It is an important health problem nowadays as it affects near 5% of the population and it has a mortality rate of about 11% [2, 3].

The standard treatment of DVT combines several concurrent elements: administration of drugs, pneumatic compression devices and prevention of immobility of the lower extremities [4]. Prevention of immobility is achieved by prescribing physical activity, usually swimming or walking, to patients with DVT. It is well known that patients feel their pain alleviated when they are physically active. Physical activity is recommended in many medical guides for DVT patients [4], and evidences of its beneficial effects are supported by a number of prospective studies [5–7]. Notwithstanding, the specific effect of the physical activity on the mechanical behavior of the thrombus is unknown.

The purpose of the present work is to assess the effects of walking on the blood flow within a thrombotic popliteal vein for a specific DVT patient. A new model that integrates solid and fluid mechanics simulations has been developed, as detailed in what follows.

2. MODEL AND METHODS

As can be seen in Figures 1 and 2, the popliteal vein is close to the semimenbranosus muscle. Consequently, a deformation of this muscle, as the one produced when walking, will cause a deformation of the popliteal vein, which in turn will influence the blood flow within the vein. To simulate the effect of this influence we developed a methodology, whose main components are sketched in Figure 3. The methodology combines three elements, namely a real geometry, a biomechanical model of body tissues and a CFD study, and it consists of three main steps.

In the first main step, labeled (I) in Figure 3, a number of axial views of CT scan images, such as the one shown in Figure 2, were used to build a 3D geometry model of a 10 cm long portion of the patient's leg. This base geometry model is a discretization of the original volume into a large number of tetrahedral cells. Each cell is categorized according to the type of tissue it represents: 1-vein, 2-semimembranosus muscle and tendon, 3-bone, 4-passive muscle, 5-soft tissue (see Figure 2).

In the second step, labeled (II) in Figure 3, we computed the deformation of the base geometry model as a function of the lengthening/shortening of the active (semimembranosus) muscle. We used a biomechanical model that assumes the semimembranosus muscle to be a hyperelastic volume-preserving fiber–reinforced composite material with transverse isotropy [8, 9]. Under these assumptions, the along–fiber lengthening (shortening) of this muscle will produce its concentric contraction (expansion) in the transversal isotropic plane in Figure 2. The level of a lengthening/shortening of the active muscle is characterized by the value of the fiber stretch parameter, λ.

Prepared using cnmauth.cls
DOI: 10.1002/cnm

Following the approaches previously reported [8–10] we characterized the deformation of the semimembranosus muscle by means of an uncoupled form of the strain energy that additively separates the dilatational (W_{vol}) and deviatoric (W_{iso}) responses of the tissue. In Refs. [8–10] two independent strain–energy functions for the muscle and the tendinous tissues were used. The place where muscle and tendon join is called myotendinous junction. The shift from muscle to tendon is characterized by a gradual transition in mechanical stiffness that minimizes stress concentration [11, 12]. We consequently defined a single strain–energy function whose deviatoric part is a parameterized addition of the muscle energy function (W^m_{iso}) and the tendon energy-function (W^t_{iso}):

$$\begin{aligned} W(X, C, a_0, \alpha) = W_{vol}(X) + W_{iso}(X, I_1, I_2, I_4, I_5) = \\ = W_{vol}(X) + \alpha(X) W^m_{iso}(X, I_1, I_2, I_4, I_5) + (1 - \alpha(X)) W^t_{iso}(X, I_1, I_2, I_4) \end{aligned} \tag{1}$$

Note that as we assume volume preservation for the semimembranosus muscle, $W_{vol}(X) = 0$ in the present study. In Eq. (1) X is the local point, C is the right Cauchy-Green deformation tensor, a_0 is the local fiber direction of the undeformed muscle and I_j are the deviatoric invariants of C defined in Table I. The superindexes m and t refer to muscle and tendinous tissue, respectively, and the function $\alpha(X)$, plotted in Figure 4, characterizes the gradual change from pure tendinous fibers to pure muscle fibers

$$\alpha(X) = A_1 \exp\left(\frac{A_2}{[d(X)]^2 - 1}\right) \tag{2}$$

Here A_1 and A_2 are constants (see Table II) and $d(X)$ is the normalized distance of X to the center of mass of the muscle ($d(X) \in [-1, 1]$). The type of tissue in position X is pure muscular (pure tendinous) when $\alpha(X) = 1$ ($\alpha(X) = 0$) (see [13] for details).

Under the above assumptions the Cauchy stress tensor σ can be written as

$$\sigma = pI + 2\left[\left(\frac{\partial W}{\partial I_1} + I_1 \frac{\partial W}{\partial I_2}\right) B - \frac{\partial W}{\partial I_2} B^2 + I_4 \frac{\partial W}{\partial I_4} a \otimes a + I_4 \frac{\partial W}{\partial I_5} (a \otimes B \cdot a + a \cdot B \otimes a)\right] \tag{3}$$

where a is the local fiber direction, p is the pressure and $B = C^T$ denotes the left Cauchy-Green deformation tensor [8, 14]. Following [8] and [9] the deviatoric parts of the strain energy for muscle and tendinous tissue were described by

$$W^m_{iso}(X, I_1, I_2, I_4, I_5) = W^m_1(I_4, I_5) + W^m_2(I_1, I_4, I_5) + W^m_3(I_4) \tag{4}$$

$$W^t_{iso}(X, I_1, I_2, I_4) = W^t_1(I_1, I_2) + W^t_2(I_4) + W^t_3(I_1, I_2, I_4) \tag{5}$$

with

$$W^m_1 = G_1\left(\frac{I_5}{I_4^2} - 1\right) \tag{6}$$

$$W^m_2 = G_2\left[cosh^{-1}\left(\frac{I_1 I_4 - I_5}{2\sqrt{I_4}}\right)\right]^2 \tag{7}$$

$$W^t_1(I_1, I_2) = \frac{C_1}{2}(I_1 - 3) + \frac{C_2}{2}(I_2 - 3) \tag{8}$$

$$W^t_3(I_1, I_2, I_4) = C_3[\exp(I_4 - 1) - I_4] \tag{9}$$

DOI: 10.1002/cnm

$$\lambda\frac{\partial W_3^m}{\partial\lambda}=\begin{cases} 9\left(\lambda/\lambda_{ofl}-0.4\right)^2 & \lambda\leq 0.6\lambda_{ofl} \\ 1-4\left(1-\lambda/\lambda_{ofl}\right)^2 & 0.6\lambda_{ofl}\leq\lambda\leq 1.4\lambda_{ofl}\end{cases} \tag{10}$$

$$\lambda\frac{\partial W_2^t}{\partial\lambda}=\begin{cases} 0 & \lambda<1 \\ C_3\left(\exp\left(C_4\left(\lambda-1\right)\right)-1\right) & 1\leq\lambda<\lambda^* \\ C_5\lambda+C_6 & \lambda\geq\lambda^*\end{cases} \tag{11}$$

In Eqs. (6)-(11) $\lambda=\sqrt{I_4}$, and G_i, C_i, λ_{ofl} and λ^* are constants whose values and physical meaning (if any) are listed in Table II.

The rest of materials labeled in Figure 2 were considered in step (II) as deformable solids, where an elastic and linear isotropic response was assumed. The values of the Young's modulus and Poisson's coefficient for each of the elastic materials are listed in Table III. The material model for the semimembranosus muscle defined by Eqs. (1)–(11) along with the Young's modulus for the rest of elements in Figure 2 and the geometry were entered to the finite element solver of the Code Aster package [15]. This software was used to compute the deformed configuration that resulted under a specific value of the fiber stretch parameter, λ. Note that this finite element code applied an iterative process to solve the nonlinear equations that yielded the deformed geometry. At each iteration step Eqs. (1)–(2) and (4)–(11) were used to update the stress field, σ, according to Eq. (3). The base geometry corresponds to $\lambda=1$, and a total of fifteen different geometries were computed, for fifteen values of λ in the range $[0.8,1.4]$, which is representative of the fiber stretch involved in walking.

In the third step of the current method, labeled (III) in Figure 3, for each of the deformed geometries the 3D mesh inside the vein region was extracted and a more refined tetrahedral mesh was built. These refined meshes were exported to the CFD solver where the Navier–Stokes and continuity equations were solved for the blood flow inside the popliteal vein. The Navier–Stokes and continuity equations for incompressible flow can be written as

$$\frac{\partial U}{\partial t}+\left(U\cdot\nabla\right)U = -\frac{1}{\rho}\nabla p+\left\{\nabla\cdot\left[\left(\frac{\mu}{\rho}\right)\nabla\right]\right\}U \tag{12}$$

$$\nabla\cdot U = 0 \tag{13}$$

where U is the flow velocity vector, ρ and μ respectively are the fluid density and viscosity and p is the pressure. In the CFD simulations we used the OpenFOAM solver [16]; details of the numerical procedure may be found elsewhere [17]. We modeled the flow of blood using both the Newtonian model, with a constant μ value in Eq. (12), and a non–Newtonian viscosity model where viscosity is a function of the local strain rate $\dot{\gamma}$. Following Fortuny et al. [17] we used the non–Newtonian Bird–Carreau model [18, 19]

$$\mu=\mu_\infty+(\mu_0-\mu_\infty)[1+(\psi\dot{\gamma})^2]^{(n-1)/2} \tag{14}$$

with $\psi=3.313$ s, $n=0.3568$, $\mu_\infty=3.45\times10^{-3}$ Pa · s and $\mu_0=0.56$ Pa · s.

DOI: 10.1002/cnm

3. RESULTS AND DISCUSSION

Fifteen different values of the fiber stretch parameter, λ, within the range $0.8 \leq \lambda \leq 1.4$ [20] were considered. Figure 5 shows two axial views of the calculated deformed geometries for values of $\lambda = 0.8$ and 1.4. Both views correspond to the same height and each particular material is denoted with a different color. The underlying computational mesh is also depicted in this figure. With the different values of λ a slight change in the area and shapes of muscles and vein can be observed, specially in the active muscle, whose transversal area becomes smaller as the fiber stretch increases, and in the passive muscle to the bottom left of Figure 5. The maximum deformation of the popliteal vein segment is found in the outlet region where the semimembranosus muscle is closer to the vein and therefore only a small part of the stress exerted by the muscle can be absorbed by soft tissue. The deformation of the vein outlet cross–section is illustrated in Figure 6 for three values of λ, namely $\lambda = 0.8$, 1 and 1.4. Note that as the semimembranosus muscle either shortens or lengthens the whole vein segment is tilted in the $x - y$ plane. Not only the shape of the vein changes with λ but, more importantly, so does the area of the vein wall and the outlet cross–section; see the computed values of these quantities in Table IV. In particular, it can be seen in Table IV that the maximum change in the vein wall area with respect to the basic undeformed state ($\lambda = 1$) is 2.8% for $\lambda = 0.8$ whereas the change in the outlet cross–section area is considerably higher, with a maximum increase of 14.6% for the largest fiber stretch level, $\lambda = 1.4$.

Figure 7 shows three instances of the blood velocity distribution at the outlet cross–section calculated for three values of the fiber stretch parameter, namely $\lambda = 0.8$, 1, and 1.4. An increase in cross–section area will result, for a given blood flow rate, in a decrease of the corresponding velocity levels. Such an effect is well reflected in the contours of Figure 7(c), $\lambda = 1.4$, where the maximum velocity levels are a 11.1% lower than those observed for the undeformed geometry ($\lambda = 1$) of Figure 7(b). It is also worth noting in Figure 7(a–c) that, as pointed out in [17], the passage of blood through the narrow gap in between the thrombus and the vein wall is a critical issue. Fortuny et al. [17] investigated the blood flow in the undeformed thrombotic popliteal vein segment, i.e., the case with $\lambda = 1$ in the current study, for several flow rates in the range $3 - 7\ \mathrm{cm}^3/\mathrm{s}$. In the present study we assumed a flow rate of $V = 5\ \mathrm{cm}^3/\mathrm{s}$ as a characteristic value on the average. Figure 8(a) shows the calculated surface–averaged WSS values at both the vein and the thrombus surfaces for all of the λ values considered. As expected, the average WSS values at the thrombus surface are always larger than the corresponding values at the vein wall. In both cases, the peak WSS values are obtained for the undeformed geometry, $\lambda = 1$, and they steadily decrease with either increasing or decreasing λ. In the case with maximum fiber stretch, $\lambda = 1.4$, such a WSS decrease reaches a 9.6% at the vein wall and a 10.8% at the thrombus surface.

To estimate the possible effects of a more intense physical exercise we also performed the CFD calculations for a flow rate of $V = 10\ \mathrm{cm}^3/\mathrm{s}$. Figure 8(b) shows the corresponding variations of the WSS levels as a function of λ. A twofold increase in V leads to an increase in WSS by a factor larger than two, in qualitative agreement with the findings of [17]. A comparison of Figure 8(a) and Figure 8(b) reveals that in spite of the disparity of WSS levels the shape of the WSS–λ profiles is almost identical for both values of the blood flow rate.

A decrease in the calculated WSS values is to be basically associated with a decrease in the maximum velocity levels which, as was discussed above, basically depend on the cross–section

DOI: 10.1002/cnm

area of the vein segment. Thus, it is important to understand the mechanisms leading to a decrease in the cross–section area for either an increase or a decrease in λ (see Table IV). It is found in the calculations that intramuscular pressure reaches values over 200 kPa, a quantity which exceeds the one of the intravenous pressure in the popliteal vein [21]. Therefore, as the muscle lengthens its transversal section decreases and the popliteal vein expands. On the contrary, as the muscle shortens its transversal section increases and the soft tissue is pushed against the popliteal vein, which in turn is displaced towards the femur (see Figures 5 and 6). However, the popliteal vein expands also in this situation as a consequence of the lesser value of Young's modulus for the soft tissue present in the area, which allows the pressed vein to expand at its expense.

Fortuny et al. [17] also showed that non–Newtonian viscosity effects were especially relevant for the lowest blood flow rates calculated. Thus, for the lowest flow rate of $V = 5\ \mathrm{cm}^3/\mathrm{s}$ the complete set of CFD calculations were also performed using the same non–Newtonian viscosity model as in [17]. The corresponding variations of the WSS levels with λ are shown in Figure 9. The relative difference in WSS values at the vein and thrombus surfaces is smaller than it is for the Newtonian fluid calculations in Figure 8(a). The WSS levels in Figure 9 are also found to decrease, with respect to the undeformed case of $\lambda = 1$, with either increasing or decreasing λ. In the case with maximum fiber stretch, $\lambda = 1.4$, such a WSS decrease reaches a 8.1% at the vein wall and a 9.8% at the thrombus surface. It is also shown in Figure 9 that the WSS decrease with increasing λ is faster for the thrombus surface than it is for the vein wall to the point that for $\lambda \geq 1.27$ the former of the two WSS curves is below the latter. Such a phenomenon, which was not observed for the Newtonian fluid calculations in Figures 8(a), (b), is most probably to be attributed to the better ability of the non–Newtonian model to characterize the curvature of flow streamlines as a result of the increased curvature of the geometry.

We have so far assumed that a constant value of the blood flow rate, V, is maintained throughout the whole walking cycle ($V = 5$ or $10\,\mathrm{cm}^3/\mathrm{s}$ for mild or intense exercise, respectively). The assumption of an average V value representative of the whole walking cycle seems reasonable but it obviates the effects of the muscle action on the blood flow rate itself. The mechanism relating skeletal–muscle actions and blood flow rate is commonly known as skeletal–muscle pump. According to the muscle pump idea, the action of skeletal muscles would produce an increase of the blood flow rate that would be roughly independent of other factors such as heart rate or arterial blood pressure.

It was found in the present CFD calculations that the drop in the WSS levels observed in Figures 8 and 9 is roughly proportional to a decrease in the calculated pressure gradient, ∇p. That is, the assumption of a constant ∇p instead of a constant V would probably imply an increase of the blood flow rate in the deformed vein geometries. In order to check if a constant ∇p will produce an increase in V we performed an additional set of CFD calculations in which we prescribed, for each of the deformed geometries in Table IV, a constant value of the pressure gradient, ∇p. In particular, we set at both the inlet and outlet vein sections the same pressure distribution that had been previously calculated for the base undeformed geometry, $\lambda = 1$, and a flow rate of $V = 5\,\mathrm{cm}^3/\mathrm{s}$. The CFD software then produced, for each particular geometry, velocity and pressure fields yielding the proper flow rate level in order to fulfill the governing equations (12) and (13). Note that the assumption of a constant ∇p along the walking cycle seems reasonable indeed for the current

DOI: 10.1002/cnm

range of values of the fiber stretching parameter, not far from $\lambda = 1$, and blood flow rates around $V = 5\ \mathrm{cm}^3/\mathrm{s}$, i.e., conditions that are characteristic of a mild exercise situation.

Figure 10 shows the calculated flow rates as a function of the active muscle stretching parameter, λ, for both the Newtonian and non–Newtonian blood viscosity models. We can see in this plot that when the active muscle shortens ($\lambda < 1$) there is only a very slight increase in V whereas as the muscle stretches ($\lambda > 1$) the blood flow rate increases more significantly up to a maximum of about 15% for $\lambda = 1.4$. Note that there is little dependence of the predicted V values on the viscosity model as the blood flow rate level is basically determined by the changes in the geometry of the vein. Figure 11 shows that the predicted V values fit well to a linear dependence with the vein outlet cross section area, i.e., the values listed in Table IV. That is, as the action of the active muscle results in an increase of the vein cross section area the blood flow rate consequently increases for a fixed level of ∇p. It is also worth noting that the dependence of the surface–averaged WSS values (not shown here) on λ in these additional calculations was rather the opposite to what is observed in Figures 8 and 9 as WSS levels were increasing/decreasing with increasing/decreasing V; notwithstanding, the observed WSS variations with λ were modest, about 5% at most.

It seems well established today that the enhancement of the blood supply (hyperemia) to skeletal muscles during exercise is primarily due to the vasodilation of blood vessels that is induced by one or several chemical agents [22, 23]. Notwithstanding, it is also commonly accepted that the skeletal–muscle action also contributes, to a lesser or higher extent depending on the particular situation, to exercise–induced hyperemia (see, e.g., [24–28]). While a detailed study of the skeletal–muscle pump phenomenon is beyond the scope of the current work we have shown that the cyclic stretching–shortening of an active muscle might result in a certain level of vasodilation which in turn would lead to some increase in blood flow rate. Note that the current results do not contradict but rather complement the notion of chemically induced hyperemia. That is, in relatively large blood vessels, such as the popliteal vein, muscle action might also produce some vasodilation and therefore partially contribute to the global hyperemia phenomenon.

4. CONCLUDING REMARKS

In this study we developed a methodology to analyze the effect of walking on both the shape of a thrombotic popliteal vein and on the blood flow inside it. In our methodology, first a set of CT images of a segment of the popliteal vein with a thrombus of a specific patient was used to reconstruct a base geometry model. Then a computational mechanical model was used to determine the deformation of the base geometry model as a function of the shortening/lengthening of the semimembranosus muscle. This computational model yielded fifteen deformed geometries which were then used in the corresponding CFD simulations to calculate the blood flow in the thrombotic area.

Note that the current methodology assumes a one–way solid fluid interaction. That is, the CFD simulations have no influence on the calculated deformations of the geometry model, as it can be seen in Figure 3. The calculated values of the pressure drop in the blood flow along the whole vein segment are about two orders of magnitude smaller than the (absolute) values of stress, $|\sigma| \approx 2 \times 10^5$ Pa, found in the region around the vein wall during the step (II) calculations (and most of such a pressure drop corresponds indeed to the contribution of the force of gravity). Thus,

DOI: 10.1002/cnm

the assumption that the solid calculations are independent of the particular state of the blood flow within the vein seems to be well founded.

Our computations showed that for a given value of the blood flow rate the WSS levels at both the thrombus and vein walls were reduced in all of the cases investigated as a result of the vein deformation (see Figures 8 and 9). That is, either a stretching or a contraction of the semimembranosus muscle would result in a reduction of drag forces at the thrombus. Notwithstanding, it is important to notice that the computed amount of reduction in WSS levels is smaller than the one resulted from the reduction in blood viscosity associated to the administration of drugs [17, 29]. Moreover, WSS is known to increase rapidly with blood flow (compare Figure 8(a) to Figure 8(b) to observe the change in WSS levels obtained in the present study). Then, walking, an activity which will be beneficial for patient's health on the overall, might produce either a decrease or an increase on WSS levels in the thrombotic vein depending on the increase of blood flow produced by a higher heart beat rate. In particular, in the current patient's case results reported by Fortuny et al. [17] suggest an increase in WSS levels at the thrombus surface according to the law $\mathrm{WSS} \propto V^{1.39}$. Thus the reduction of 10.8% in Figure 8(a) will be counterbalanced by an increase in blood flow rate of just a 5.5%. Indeed, it would appear that the effects of walking on the blood flow will be patient–specific. The methodology described in this paper provides the framework for the development of an automated process that will help physicians to tailor medical recommendations and treatments to each specific patient.

In addition, we also carried out a set of CFD calculations in which the pressure drop between the inlet and outlet vein sections was fixed so that a different value of the blood flow rate was obtained for each particular deformed geometry model. It was observed in these calculations that an increase of the vein volume induced by the action of the muscle resulted in a slight increase (15% at most) of the blood flow rate. This result suggests a future line of investigation on the effects of the application of compression devices in thrombotic veins. Just like a shortening–lengthening of the muscle changes the geometry of both the area around the vein and the vein itself, and this change results in a significant modification of WSS and V levels, applying a permanent or a pneumatic compression through external devices may produce a similar effect. The changes in the geometry model and the resulting variations of the WSS levels would then be computed for a given distribution of the external pressure exerted on the leg.

ACKNOWLEDGEMENT

Financial support for the current research was granted by Universitat Rovira i Virgili, project number 2014PFR-URV-B2-66.

REFERENCES

1. White RH. The epidemiology of venous thromboembolism. *Circulation* 2003; **107**:14–18.
2. Cushman M, Tsai AW, White RH, Heckbert SR, Rosamond WD, Enright P, Folsom AR. Deep vein thrombosis and pulmonary embolism in two cohorts: The longitudinal investigation of thromboembolism etiology. *Am. J. Med.* 2004; **117**:19–25, doi:10.1016/j.amjmed.2004.01.018.

DOI: 10.1002/cnm

3. Cohen AT, Agnelli G, Anderson FA, Arcelus JI, Bergqvist D, Brecht JG, Greer IA, Heit JA, Hutchinson JL, Kakkar AK, *et al.*. The number of VTE events and associated morbidity and mortality. *J. Thrombosis Haemostasis* 2007; **98**:756–764, doi:10.1160/TH07030212.
4. Kearon C, Akl EA, Comerota AJ, Prandoni P, Bounameaux H, Goldhaber SZ, Nelson ME, Wells PS, Gould MK, Dentali F, *et al.*. Antithrombotic therapy for VTE disease: Antithrombotic therapy and prevention of thrombosis, 9th ed: American college of chest physicians evidence-based clinical practice guidelines. *Chest* 2012; **141**(2):e419S–e494S, doi:10.1378/chest.11-2301.
5. Chandra D, Parisini E, Mozaffarian D. Meta-analysis: Travel and risk for venous thromboembolism. *Annals of Internal Medicine* 2009; **151**(3):180–190, doi:10.7326/0003-4819-151-3-200908040-00129.
6. Kahn SR, Shrier I, Kearon C. Physical activity in patients with deep venous thrombosis: A systematic review. *Thrombosis Research* 2008; **122**(6):763 – 773, doi:10.1016/j.thromres.2007.10.011.
7. Frey PM, Méan M, Limacher A, Jaeger K, Beer HJ, Frauchiger B, Aschwanden M, Rodondi N, Righini M, Egloff M, *et al.*. Physical activity and risk of bleeding in elderly patients taking anticoagulants. *Journal of Thrombosis and Haemostasis* 2015; **13**(2):197–205, doi:10.1111/jth.12793.
8. Weiss JA, Maker BN, Govindjee S. Finite element implementation of incompressible, transversely isotropic hyperelasticity. *Computer Methods in Applied Mechanics Engineering* 1996; **135**:107–128.
9. Blemker SS, Pinsky PM, Delp SL. A 3d model of muscle reveals the causes of nonuniform strains in the biceps brachii. *Journal of Biomechanics* 2005; **38**:657–665.
10. Simo JC, Taylor RL. Quasi–incompressible finite elasticity in principal stretches: continuum basis and numerical examples. *Computer Methods in Applied Mechanics Engineering* 1991; **51**:273–310.
11. Guilak F, Butler D, Goldstein S, Mooney e DJ. *Functional Tissue Engineering*. Springer-Verlag: New York, 2003.
12. Standring S. *Gray's Anatomy: The Anatomical Basis of Clinical Practice, 41st Edition*. Elsevier: Philadelphia, 2015.
13. Toumanidou T, Noailly J, Puigjaner D, Fortuny G. A continuum model for the whole muscle. *Journal of Biomechanics* 2012; **45**(S1):S484. 18th Congress of the European Society of Biomechanics. Topic 34. Muscle biomechanics.
14. Holzapfel GA. *Nonlinear Solid Mechanics. A Continuum Approach for Engineering*. John Wiley & Sons: Chichester, 2000.
15. EDF. Code-Aster: Analysis of Structures and Thermomechanics for Studies & Research. `http://www.code-aster.org` 2015. [Online; accessed 25-May-2015].
16. The OpenFOAM Foundation. `http://openfoam.org/` 2015. [Online; accessed 25-May-2015].
17. Fortuny G, Herrero J, Puigjaner D, Olivé C, Marimon F, Garcia-Bennet J, Rodríguez D. Effect of anticoagulant treatment in deep vein thrombosis: a patient-specific computational fluid dynamics study. *Journal of Biomechanics* 2015; doi:10.1016/j.jbiomech.2015.03.026. Accepted for publication. doi 10.1016/j.jbiomech.2015.03.026.
18. Bird RB, Amstrong RC, Hassager O. *Dynamics of Polimeric Liquids*. Second edn., John Wiley & Sons: New York, 1987.
19. Cho YI, Kensey KR. Effects of the non–Newtonian viscosity of blood on flows in a diseased arterial vessel. Part 1: steady flows. *Biorheology* 1991; **28**(3–4):241–262.
20. Huxley AF. Muscular contraction. *J Physiol-London* 1974; **243**(1):1–43.
21. Neglén P, Raju S. Differences in pressures of the popliteal, long saphenous, and dorsal foot veins. *Journal of Vascular Surgery* 2000; **32**(5):894–901, doi:10.1067/mva.2000.110351.
22. Mortensen SP, Saltin B. Regulation of the skeletal muscle blood flow in humans. *Exp. Physiol.* 2014; **99**:1552–1558, doi:10.1113/expphysiol.2014.081620.
23. Joyner MJ, Casey DP. Regulation of increased blood flow (hyperemia) to muscles during exercise: A hierarchy of competing physiological needs. *Physiol. Rev.* 2015; **95**:549–601, doi:10.1152/physrev.00035.2013.
24. Shiotani I, Sato H, Sato H, Yokoyama H, Ohnishi Y, Hishida E, Kinjo K, Nakatani D, Kuzuya T, Hori M. Muscle pump-dependent self-perfusion mechanism in legs in normal subjects and patients with heart failure. *J. Appl. Physiol.* 2002; **92**:1647–1654, doi:10.1152/japplphysiol.01096.2000.
25. Tschakovsky ME, Sheriff DD. Immediate exercise hyperemia: contributions of the muscle pump vs. rapid vasodilation. *J. Appl. Physiol.* 2004; **97**:739–747, doi:10.1152/japplphysiol.00185.2004.
26. Lutjemeier BJ, Miura A, Scheuermann BW, Koga S, Townsend DK, Barstow TJ. Muscle contraction-blood flow interactions during upright knee extension exercise in humans. *J. Appl. Physiol.* 2005; **98**:1575–1583, doi: 10.1152/japplphysiol.00219.2004.
27. McDaniel J, Hayman MA, Ives S, Fjeldstad AS, Trinity JD, Wray DW, Richardson RS. Attenuated exercise induced hyperaemia with age: mechanistic insight from passive limb movement. *J. Physiol.* 2010; **588**:4507–4517, doi: 10.1113/jphysiol.2010.198770.

DOI: 10.1002/cnm

28. Sheriff DD. Role of mechanical factors in governing muscle blood flow. *Acta Physiol*. 2010; **199**:385–391, doi: 10.1111/j.1748-1716.2010.02120.x.
29. Marimon F, López JM, Fortuny G, Herrero J, Puigjaner D. Influence of anticoagulant treatment on blood viscosity in patients with venous thromboembolism 2016; In preparation.
30. Chen E, Novakofski J, Jenkins W, O'Brien J WD. Young's modulus measurements of soft tissues with application to elasticity imaging. *Ultrasonics, Ferroelectrics, and Frequency Control, IEEE Transactions on* Jan 1996; **43**(1):191–194, doi:10.1109/58.484478.
31. Comley K, Fleck NA. A micromechanical model for the youngs modulus of adipose tissue. *Int J Solids Struct* 2010; **47**:2982–2990.
32. Wesly RLR, Vaishnav RN, Fuchs JCA, Patel DJ, Greenfield JC. Static linear and nonlinear elastic properties of normal and arterialized venous tissue in dog and man. *Circulation Research* 1975; **37**:509–520.
33. Stålhand J. Determination of human arterial wall parameters from clinical data. *Biomech Model Mechanobiol* 2009; **8**:141–148, doi:10.1007/s10237-008-0124-3.

DOI: 10.1002/cnm

Table I. Definition of the deviatoric invariants for the right Cauchy-Green deformation tensor C.

Invariant	Definition
I_1	trC
I_2	$\frac{1}{2}\left[(trC)^2 - trC^2\right]$
I_4	$a_0 C a_0 = \lambda^2$
I_5	$a_0 C^2 a_0$

DOI: 10.1002/cnm

Table II. Values and physical meaning (if any) of the constants involved in the model described by Eqs. (1)–(11).

Constant	Physical meaning	Value	Reference
G_1	along-fiber shear modulus	5×10^2 Pa	
G_2	cross-fiber shear modulus	5×10^2 Pa	
C_3		2.7×10^6 Pa	
C_4	rate of uncrimping of the collagen fibers	46.4	[9]
C_5		$5.\times10^8$ Pa	
C_6		-5.1×10^8 Pa	
λ_{ofl}	optimal fiber stretch	1.4	
λ^*	fiber stretch at which the collagen fibers are straightened	1.03	
C_1		1.385×10^7 Pa	[8]
C_2		0	
A_1		1.105	
A_2		0.1	

DOI: 10.1002/cnm

Table III. Values of the Young's modulus and Poisson's coefficient for each of the elastic materials.

Material	Young's modulus	Poisson's coefficient	Reference
Bone tissue	12 GPa	0.3	[30]
Passive muscle	3 kPa	0.45	[30]
Soft tissue	1 kPa	0.45	[31]
Popliteal vein	2 kPa	0.45	[32, 33]

DOI: 10.1002/cnm

Table IV. Calculated surface area and outlet cross section of the popliteal vein for fifteen instances of the fiber stretch parameter λ.

λ	Vein wall area (cm^2)	Outlet cross–section area (cm^2)
0.80	26.23	1.23
0.87	26.21	1.21
0.94	26.20	1.20
1.00	26.19	1.18
1.06	26.30	1.19
1.10	26.32	1.19
1.13	26.40	1.21
1.14	26.43	1.22
1.16	26.47	1.23
1.19	26.52	1.24
1.21	26.59	1.26
1.23	26.65	1.27
1.27	26.72	1.29
1.32	26.81	1.32
1.40	26.93	1.36

DOI: 10.1002/cnm

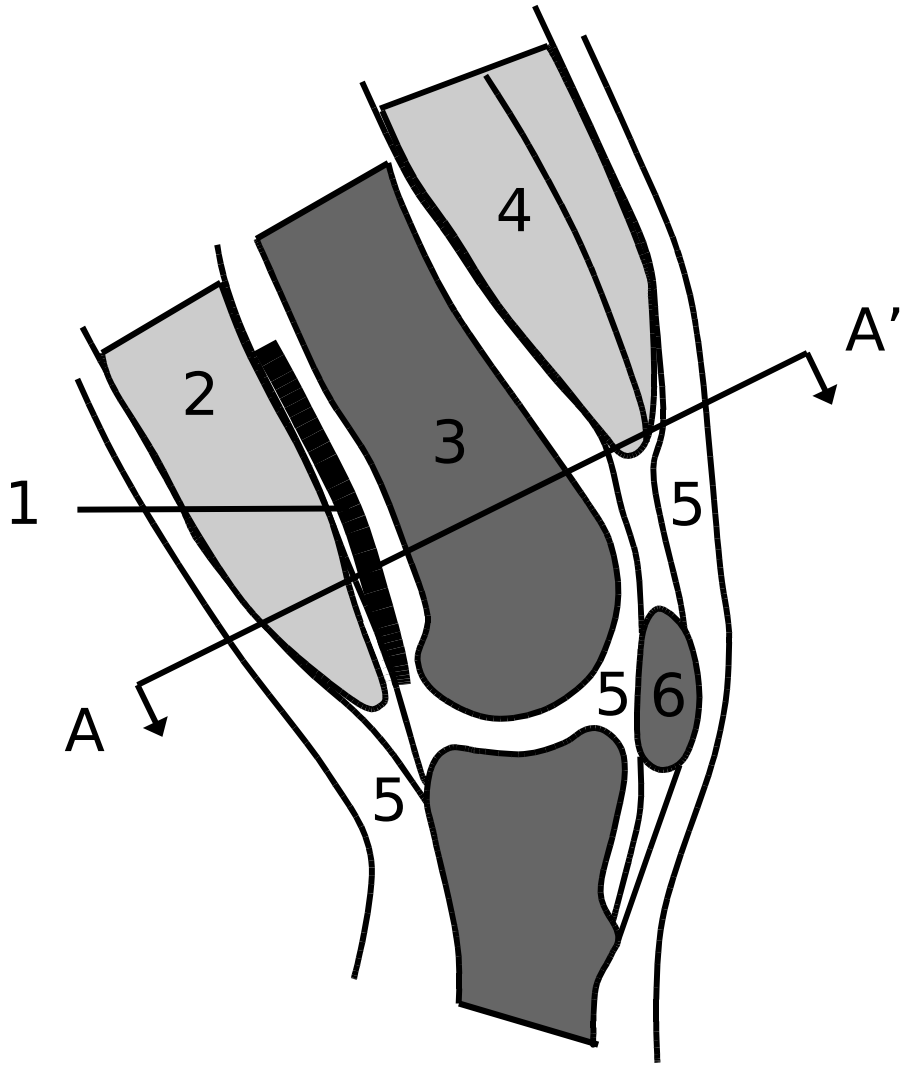

Figure 1. Sketch of a sagital section around the knee showing elements that are relevant to the current problem: (1) segment investigated of the popliteal vein , (2) active muscle (semimembranosus) and tendon, (3) femur, (4) passive muscles (here quadriceps muscles), (5) soft tissue, (6) knee cap. The A–A' line denotes the particular cross-section corresponding to the axial CT image which is shown in Figure 2.

Prepared using cnmauth.cls
DOI: 10.1002/cnm

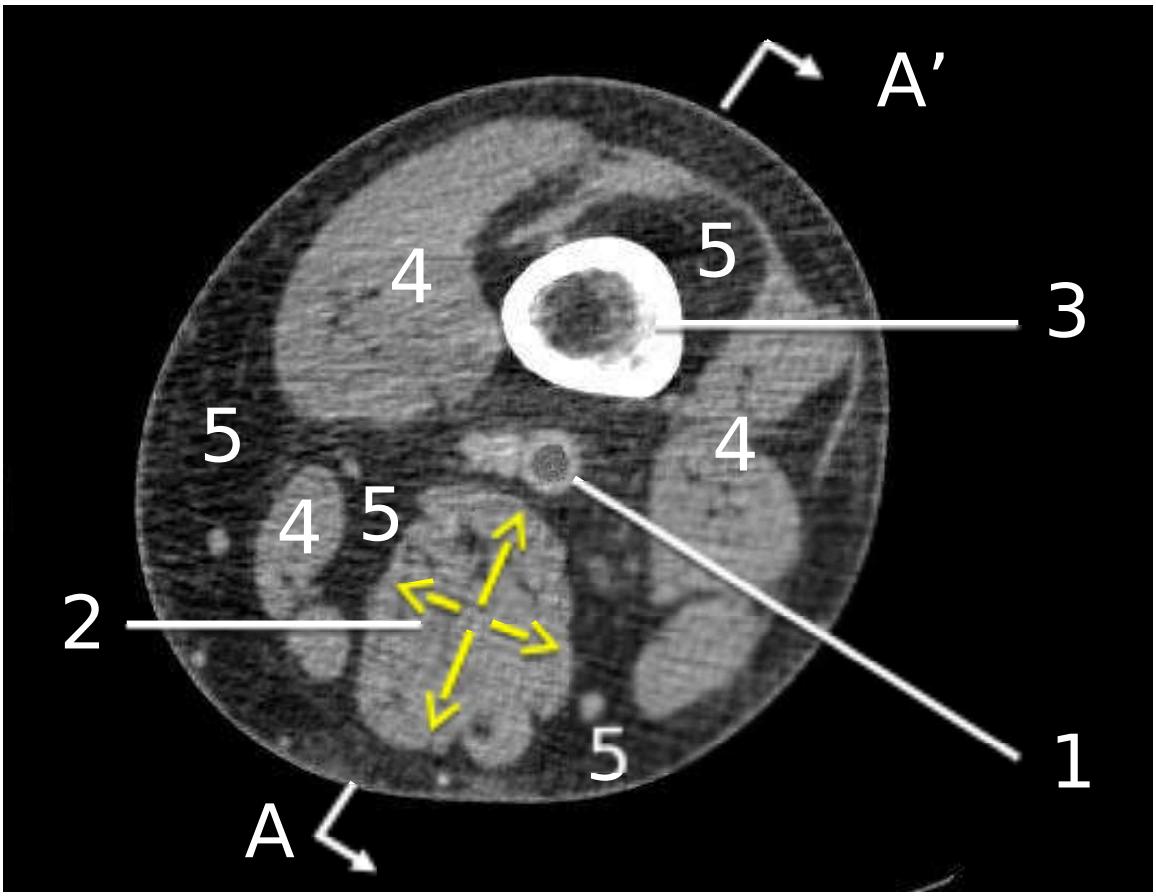

Figure 2. Computerized tomography (CT) image corresponding to an axial view above the knee. The 1–5 labels, consistent with the ones used in Figure 1, denote: (1) popliteal vein with a thrombus, (2) active (semimembranosus) muscle, (3) femur, (4) passive muscles, (5) soft tissue. The arrows plotted in the active (semimembranosus) muscle represent the concentric expansion produced by an along–fiber shortening of this muscle.

DOI: 10.1002/cnm

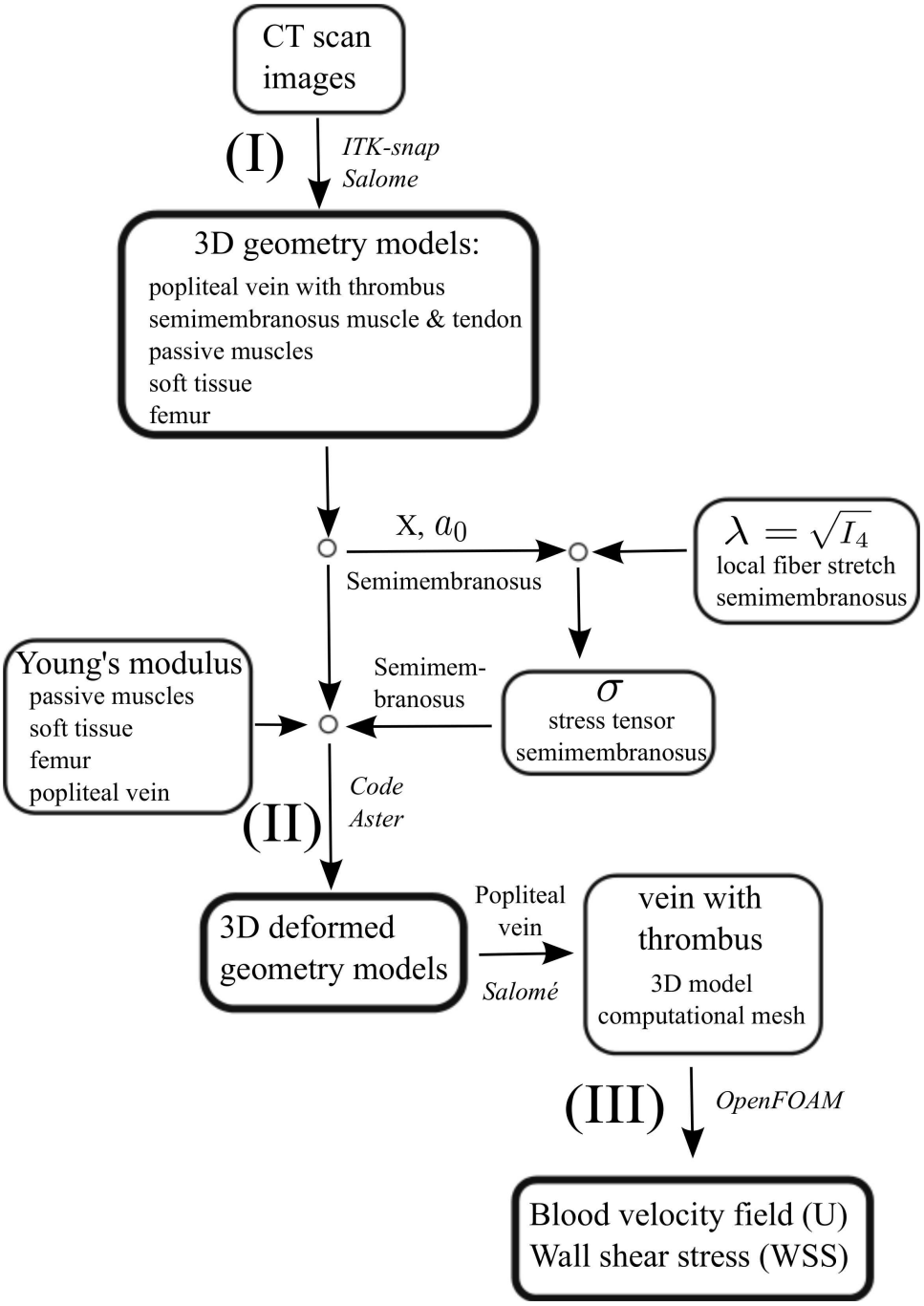

Figure 3. Flow diagram of the developed methodology illustrating which data and parameters were taken as initial inputs, which steps were followed and which models and software were used.

DOI: 10.1002/cnm

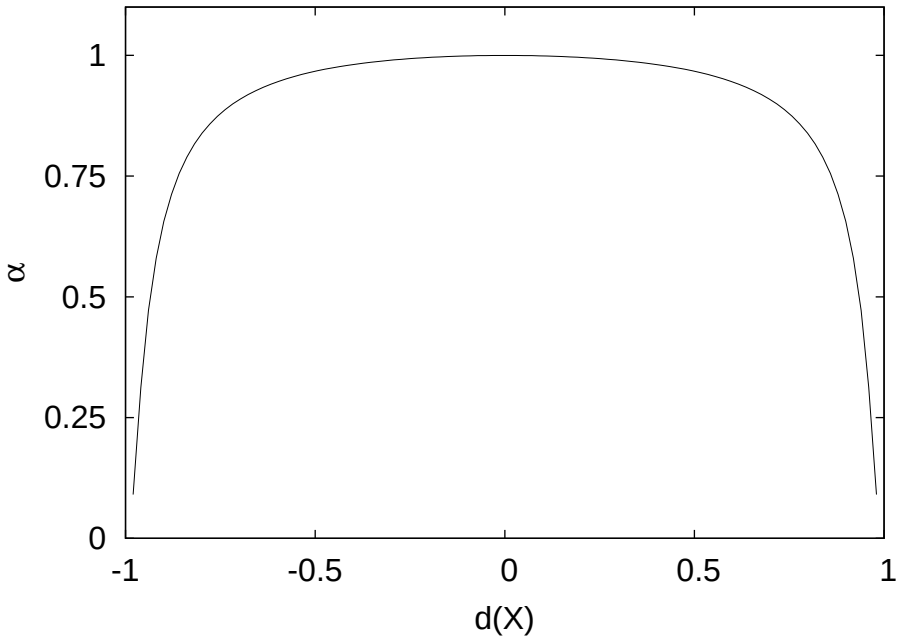

Figure 4. Plot of the tendon–muscle transition function, $\alpha(X)$, defined in Eq. (2). The limiting values $\alpha = 0$ and $\alpha = 1$ respectively correspond to pure tendinous tissue and pure muscular tissue.

DOI: 10.1002/cnm

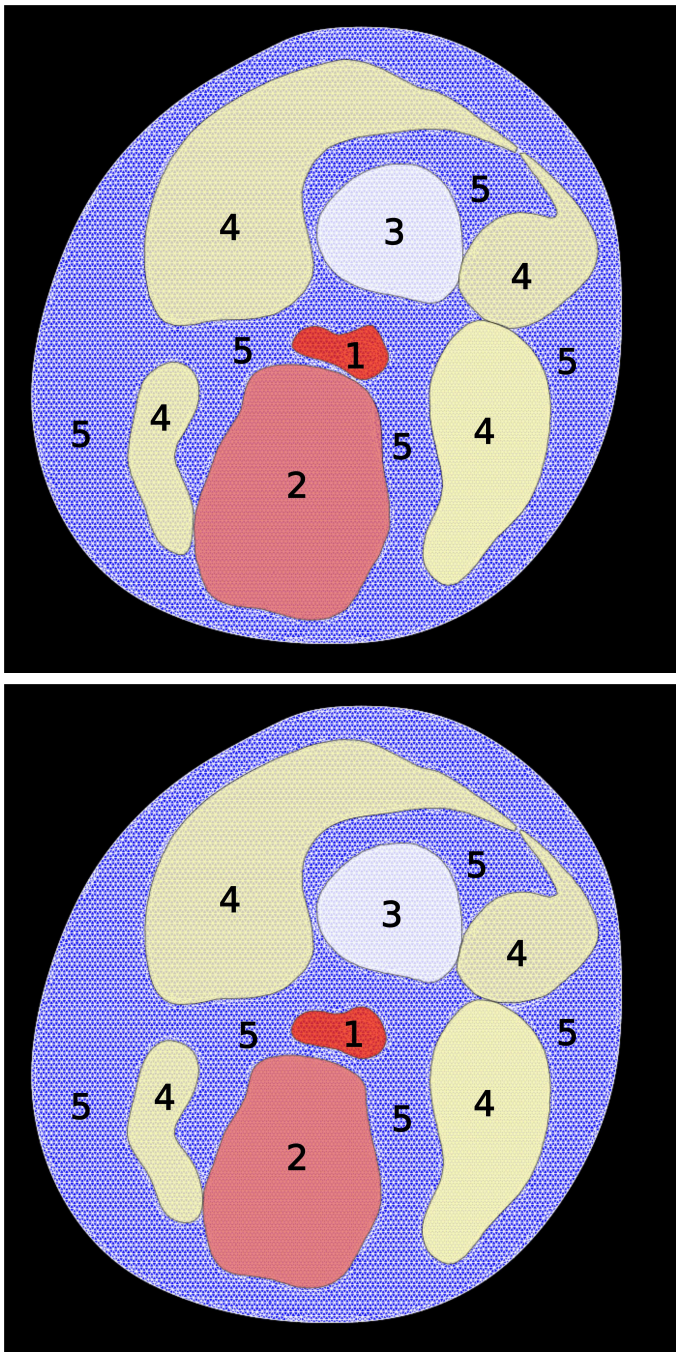

Figure 5. Axial view of the calculated deformed geometries for two values of the fiber stretch parameter $\lambda = 0.8$ and 1.4. See Figure 2 for the meaning of labels.

DOI: 10.1002/cnm

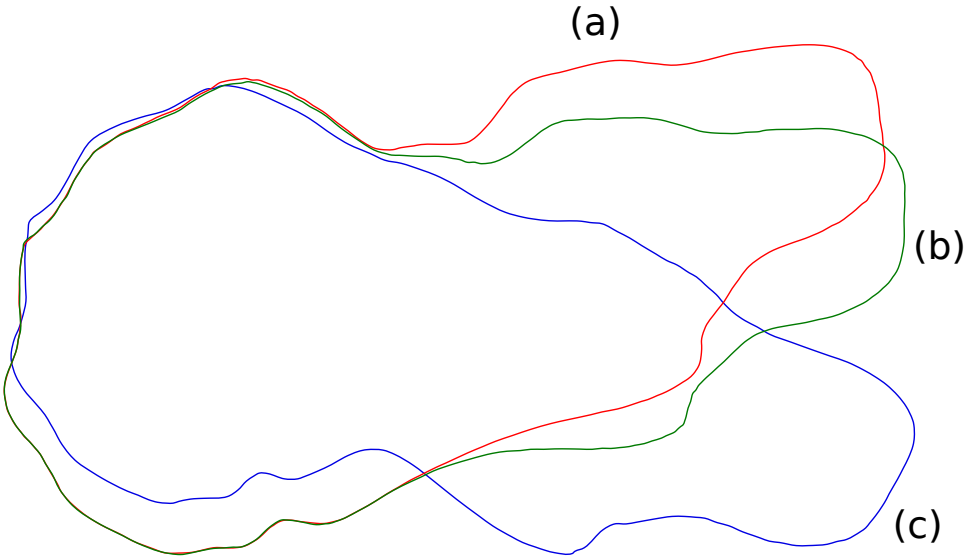

Figure 6. Perimeter of the vein outlet cross–section in three cases with: a) minimum value of fiber stretch ($\lambda = 0.8$), b) non–deformed geometry ($\lambda = 1$), c) maximum value of fiber stretch ($\lambda = 1.4$).

DOI: 10.1002/cnm

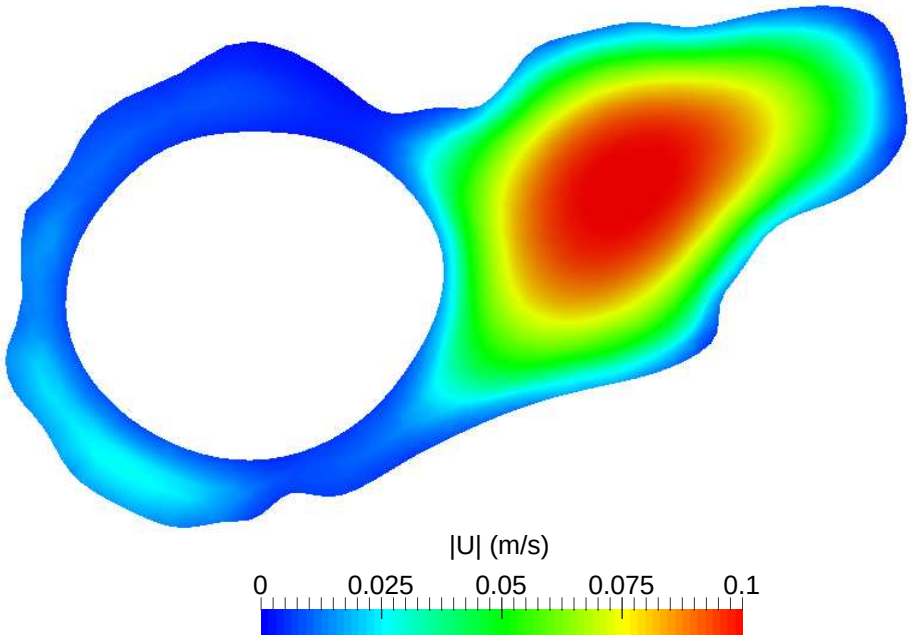

a)

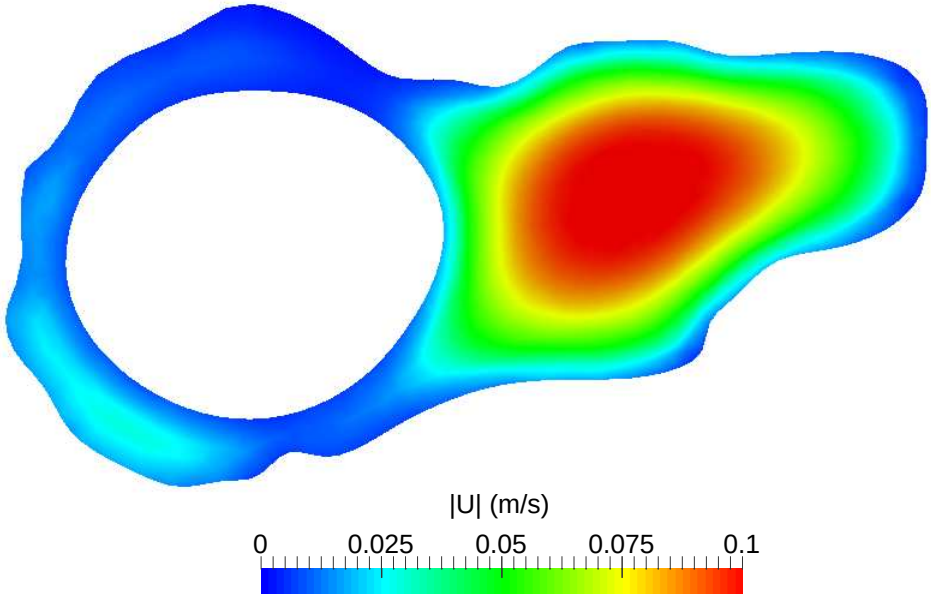

b)

DOI: 10.1002/cnm

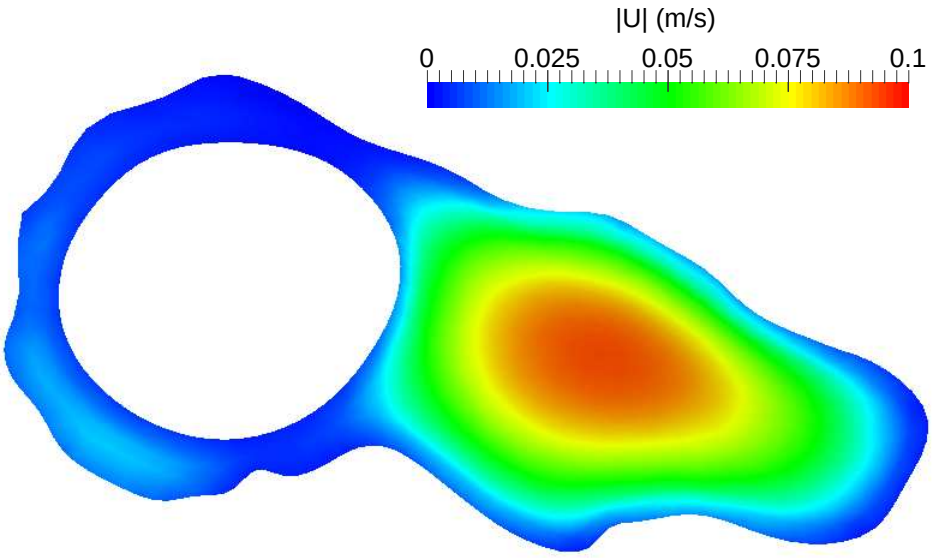

c)

Figure 7. Outlet velocity distributions calculated using the non–Newtonian viscosity model for a blood flow rate of $5\ \mathrm{cm}^3/\mathrm{s}$ in the cases with: a) minimum value of fiber stretch ($\lambda = 0.8$), b) non–deformed geometry ($\lambda = 1$), and c) maximum value of fiber stretch ($\lambda = 1.4$).

DOI: 10.1002/cnm

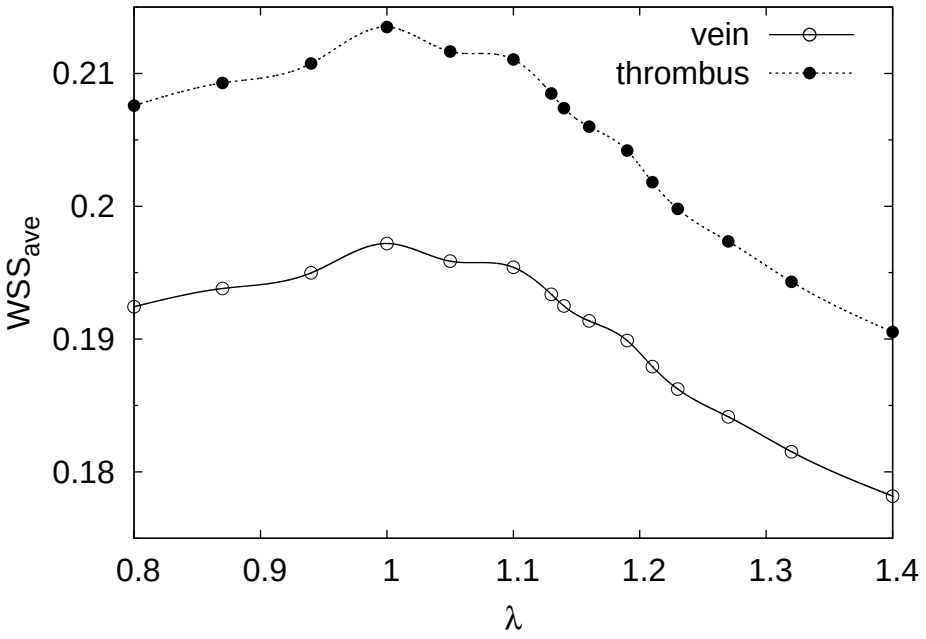

a)

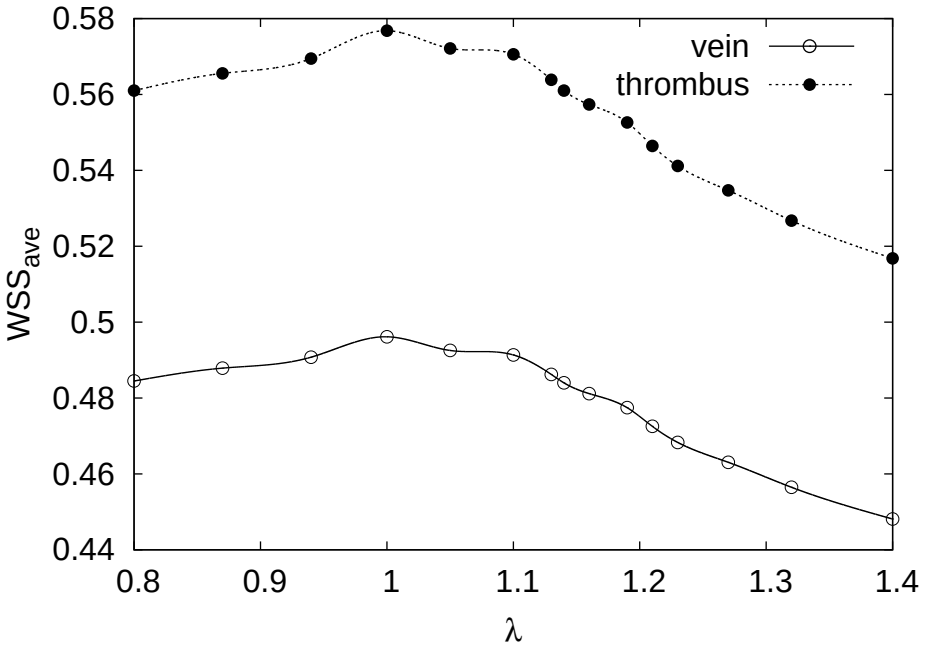

b)

Figure 8. Variation with λ of the average WSS levels at the vein and thrombus walls for the calculations with the Newtonian viscosity model and blood flow rate of (a) $V = 5\ \mathrm{cm}^3/\mathrm{s}$ and (b) $V = 10\ \mathrm{cm}^3/\mathrm{s}$.

Prepared using cnmauth.cls
DOI: 10.1002/cnm

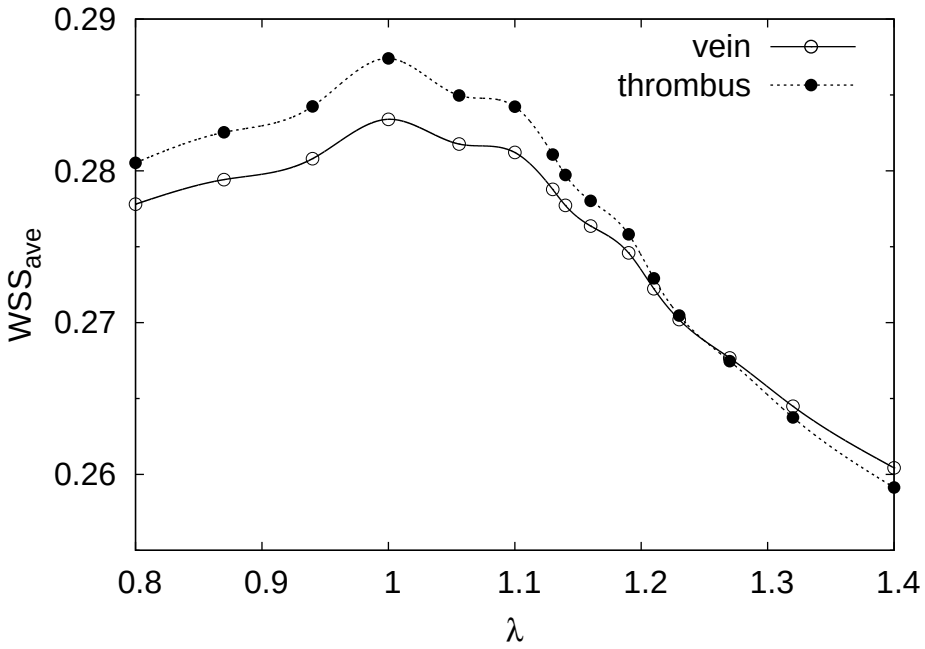

Figure 9. Variation with λ of the average WSS levels at the vein and thrombus walls for the calculations with the non–Newtonian viscosity model and a blood flow rate of $V = 5\ \mathrm{cm}^3/\mathrm{s}$

.

DOI: 10.1002/cnm

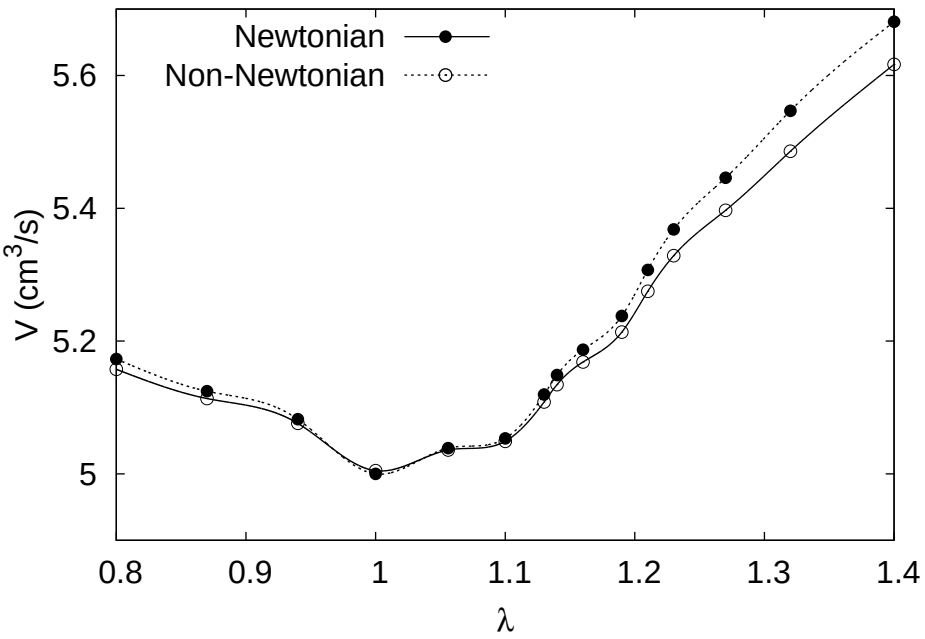

Figure 10. Values of the calculated blood flow rate, V, as a function of the active muscle stretching parameter, λ, for two sets of calculations with either the Newtonian and the non–Newtonian viscosity models. In each set of calculations, a unique pressure distribution is prescribed at the inlet and outlet vein sections such that the reference $V = 5\ \mathrm{cm}^3/\mathrm{s}$ level is obtained for the base geometry with $\lambda = 1$.

DOI: 10.1002/cnm

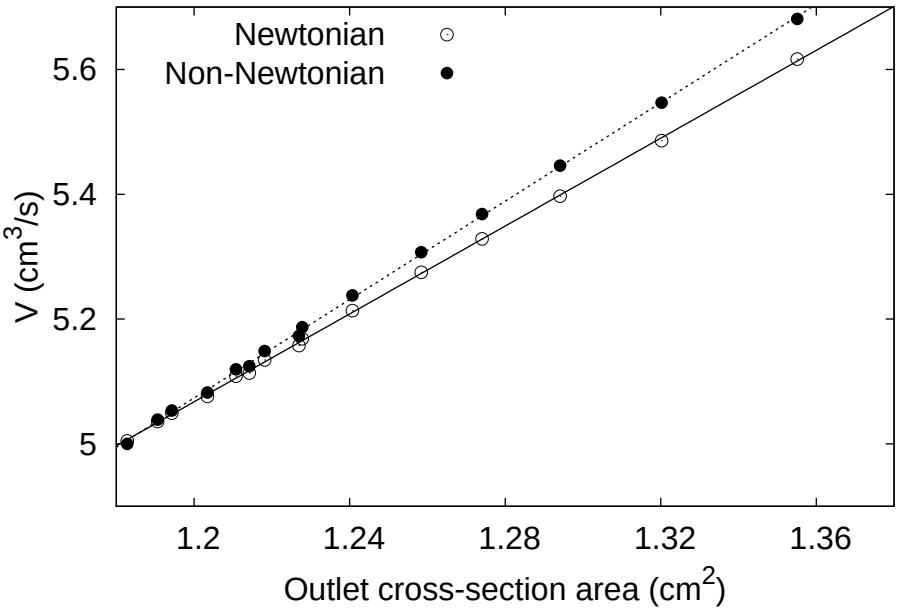

Figure 11. Linear fit of the V values of Figure 10 as a function of the corresponding area at the vein outlet cross–section, A, whose values are shown in Table IV. The fit equations are $V = 3.52A + 0.84$ and $V = 3.94A + 0.34$ for the Newtonian and non–Newtonian calculations, respectively.

DOI: 10.1002/cnm